4.4 Results

This final section may be regarded as the most significant portion of the dissertation. First, we present a typical case of pre-analysis data, giving an example of what one sees during an experiment. Next, we go directly to momentum space, and give examples of the conservation in the longitudinal direction. Finally, we will present a variety of spectra in transverse momentum for three different collision systems.

4.4.1 Raw Data

We begin the presentation of the experimental results with an example of raw data. Presented in figures 4.8 and 4.9 are the raw data for the reoil ions and soft electrons produced by the collision system 1 MeV/amu F^{9+} + He. Figure 4.8 shows the raw data corresponding to the recoil ion measurement, while figure 4.9 shows similar spectra corresponding to the electron measurement. In each figure, the spectrum at lower left is the density plot of the position on the detector, with projections across and up plotted immediately to the right and above respectively. The histograms of the signals from the time to amplitude converters (TAC_e and TAC_{eR}) are plotted in the upper right of both figures.

There are two features to note in the recoil position spectrum. Recoil ions originating from the gas jet can be seen as a very intense spot on the 2-d

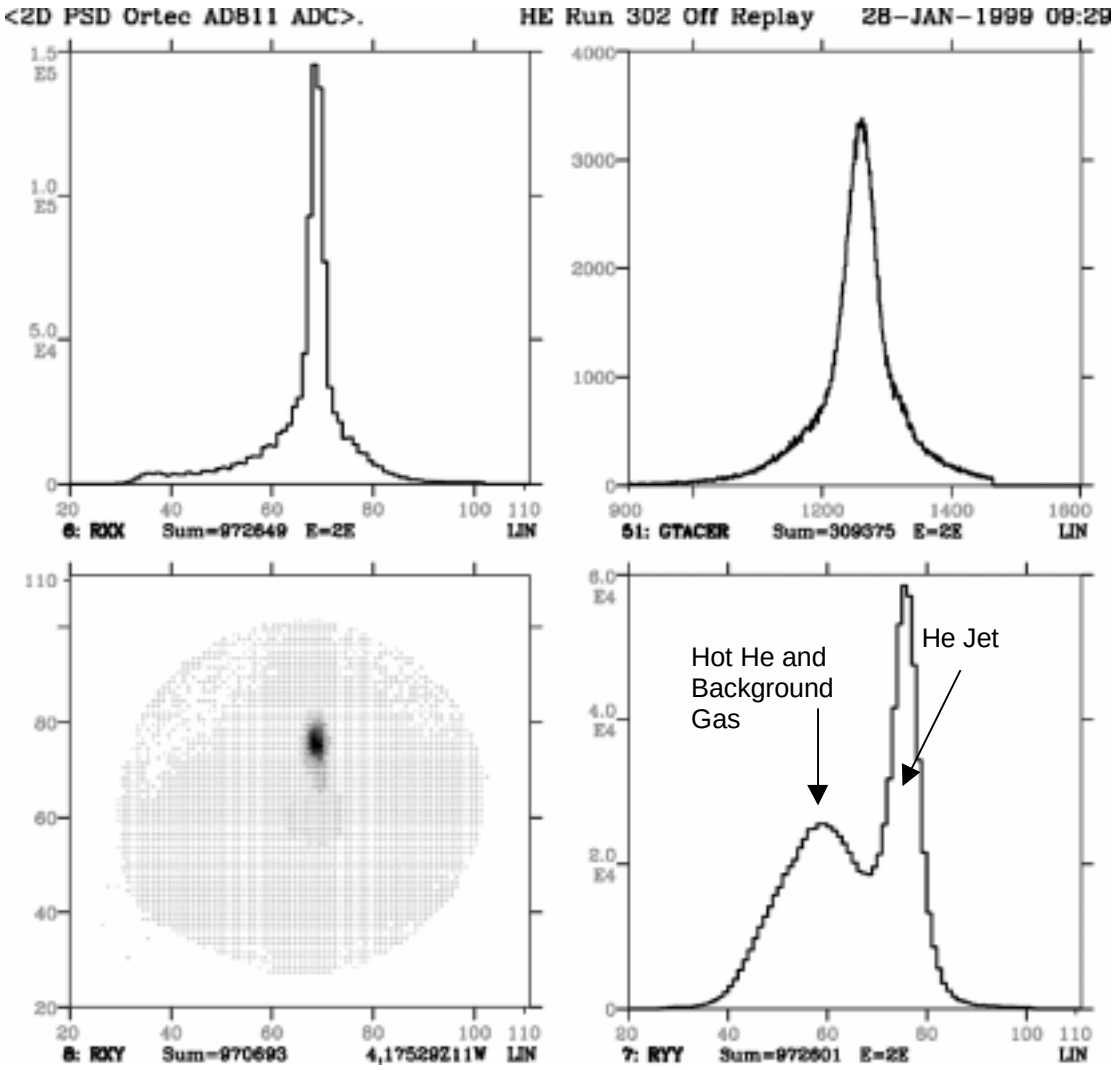

Figure 4.8: Raw recoil ion spectra for 1 MeV/amu bare flourine colliding with helium. Lower left is the detector image with projections immediately above and to the right. Upper right is the electron-recoil (TACeR) time of flight distribution used for calculating P_{Rx}.

spectrum, and in the projections as the prominent tall peak. Recoil ions originating from hot (room temperature) helium and background gases appear in the faint blob below the jet position. Although produced along the length of the ion beam within the spectrometer, the hot gas distribution does not cover the entire length of the detector because the hot gas is spatially focused as well. The hot gas peak is quite visible in the projection across the detector. Remembering that the position on the recoil detector is directly proportional to momentum, one can see that the momentum distribution of the hot gas is much broader than that of the jet. This is due to the large thermal spread in the hot gas, compared to that in the supersonically cooled jet.

In figure 4.9, we see the 2-d electron position spectrum along with its corresponding projections. While not directly proportional as in the recoil case, the electron position is an indication of the momentum along the z- and y- axis. This particular collision system is 1 MeV/amu F^{9+} + He, and a strong post-collision interaction can be seen pulling the electrons toward the left (the beam goes from right to left in the figure). There is also an underlying background (in this case unfocused) due to the interaction between the ion beam and the hot gas along the length of the electron detector. In the projection across, the cylindrical geometry defined by the beam axis is evident in the symmetry of the distribution.

The spectrum at the upper right of both figures is a histogram of the raw time to amplitude converter (TAC_{eR} and TAC_e) signals. The recoil TAC_{eR} is a measure of the time difference between the electron signal (start) and recoil signal (stop), whereas the electron TAC is the time difference between the electron signal (start) and the

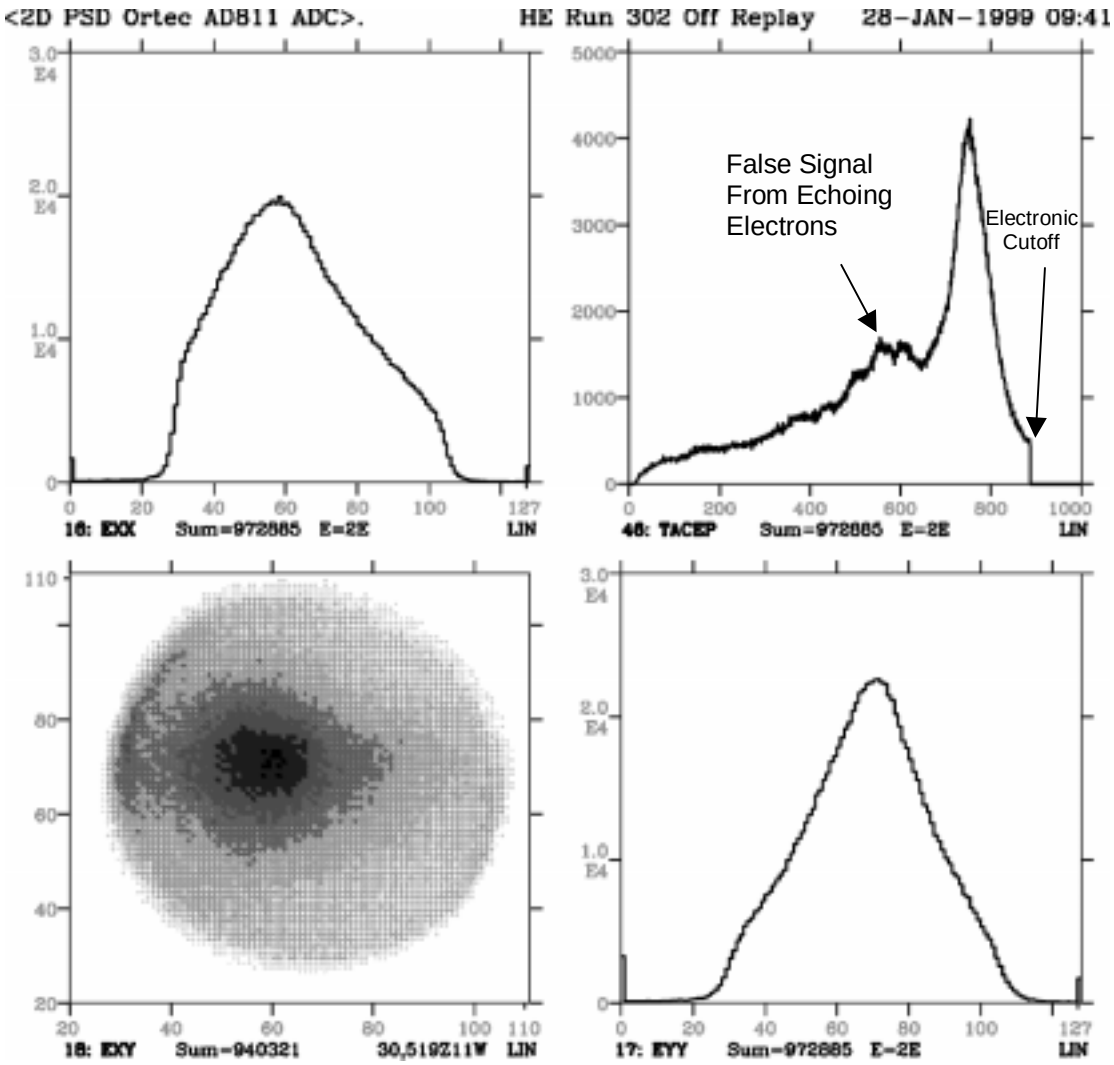

Figure 4.9: Raw electron spectra for 1 MeV/amu bare fluorine colliding with helium. Lower left is the detector image with projections immediately above and to the right. Upper right is the recoil time of flight distribution used for calculating P_x.

projectile bunch clock (stop). By converting both spectra from channels to nanoseconds, the electron and recoil times of flight (TOF) may be determined. In the present case, the conversions are 18.82 ± 0.02 ch/nsec for the TAC_e (electron) and 9.14 ± 0.03 ch/nsec for the recoil TAC_{eR} (electron-recoil). The TACs were calibrated using a pulser for a start and the same signal delayed for a stop; by incrementing the delay a known amount, a calibration spectrum was generated.

4.4.2 Longitudinal Momentum

As explained previously, the longitudinal momentum transfer in the collision is governed by a combination of conservation laws and post-collisional effects. Therefore a strong correlation must exist between the recoil and electron longitudinal momenta. Figures 4.10 and 4.11 illustrate this point. Shown in the upper portion of figure 4.10 is a density plot of the correlation between the electron and recoil longitudinal momentum for the collision system 1 MeV H^+ + He. The 45° line corresponds to an exact balance between the electron and recoil. The data must be offset from this line by the momentum loss of the projectile. In order to ionize the helium, the projectile must lose energy (eq. 4.5). For the present case, typical energy transfers of about 1 a.u. would correspond to shift of 0.16 a.u., which agrees with our data. In addition, there is a clear correlation between the electron and recoil longitudinal momentum.

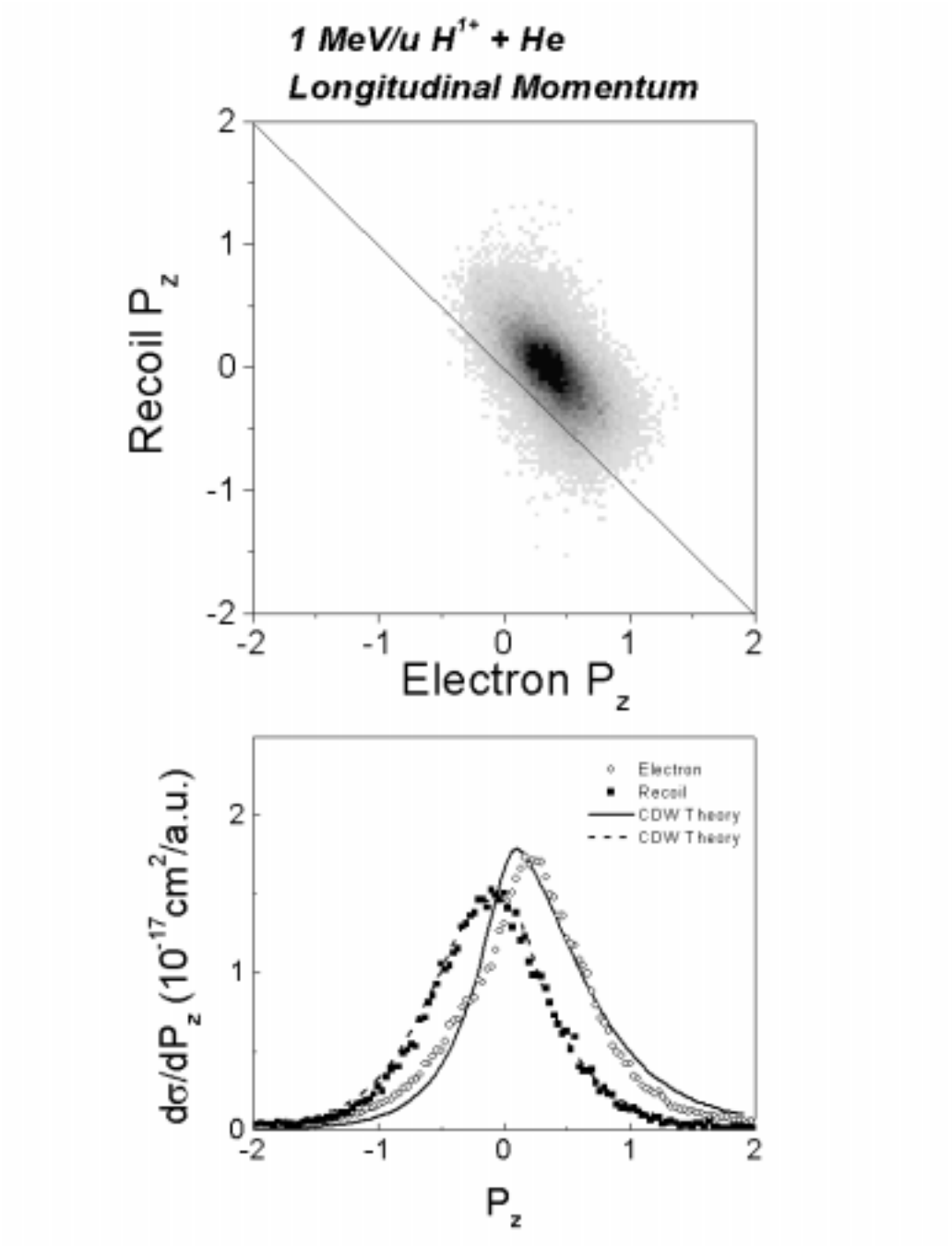

Figure 4.10: Density plot (top) of the doubly differential cross section $d^2\sigma/dP_{ZR}\,dP_{Ze}$. and (bottom) singly differential cross sections $d\sigma/dP_{Ze}$ and $d\sigma/dP_{ZR}$ for the collision system 1 MeV H^+ + He. The curves are CDW theory.

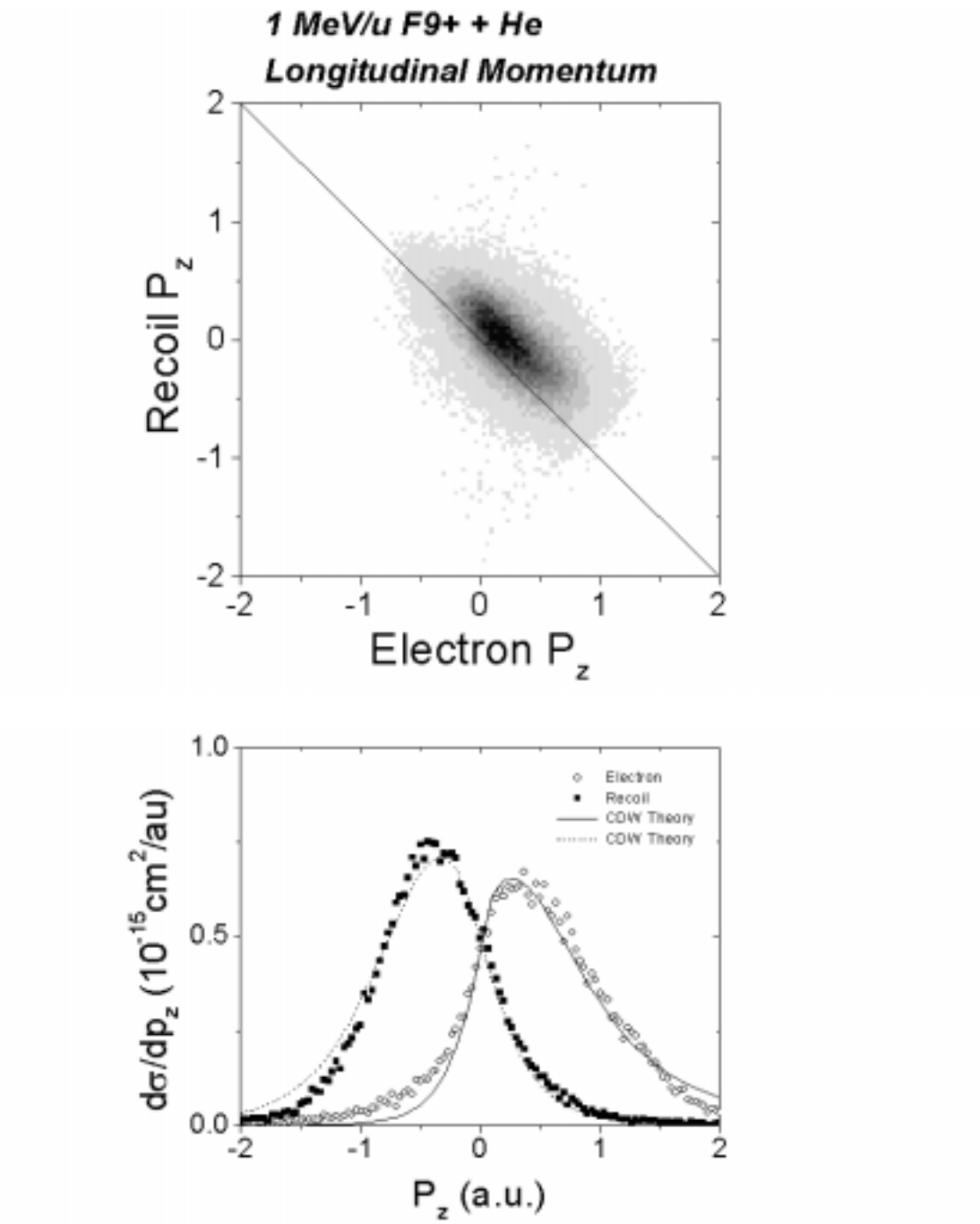

Figure 4.11: Density plot (top) of the doubly differential cross section $d^2\sigma/dP_{ZR}\,dP_{Ze}$. and (bottom) singly differential cross sections $d\sigma/dP_{Ze}$ and $d\sigma/dP_{ZR}$ for the collision system 1 MeV/amu F^{9+} + He. The curves are CDW theory.

The cross sections singly differential in P_z are presented below the density plots. The data were normalized to the CDW theory. The theory and experiment agree quite well. This is not surprising. CDW theory takes into account the electron-projectile interaction as well as the electron-recoil interaction. Due to the restrictions on the kinematics in the longitudinal direction (eq. 4.7), the calculation is able to sufficiently represent the data. In the transverse case which will be discussed later, the projectile-recoil interaction must considered in calculations; this is because the kinematic restriction doesn't apply for the transverse momentum exchanges. Note that the electron longitudinal momentum distribution is more positive (beam direction) than that of the recoils, as expected by interaction with the receding beam (post-collision effect).

Figure 4.11 show the same spectra for the 1 MeV/amu F^{9+} + He system. The result is similar, except for the increased separation of the peaks in the 1-d spectrum, indicating a stronger post-collision interaction. Again, the data were normalized to the theory, and agree reasonably well. Similar measurements of the 3.6 MeV/u Se^{28+} +He system by Moshammer *et al*. [4.11] also show good agreement with CDW caculations. Furthermore, this information can be extracted measurements of the electron distributions in energy and angle. Tribedi *et al*. [2.2] did this for the 2.5 MeV/u C^{6+} + He system, and the resultant distributions were used to compare with our measurements described in chapter 2. These measurements were also in good agreement with CDW theory.